

Wind wave growth at short fetch

T. Lamont-Smith¹ and T. Waseda

Ocean and Environmental Engineering Department, University of Tokyo

¹ Currently with QinetiQ (Ltd.), Malvern, UK

4 July 2006, revised May 2007

Corresponding author:

T. Lamont-Smith

Bernard Lovell Building

QinetiQ

St Andrew's Road

Malvern

Worcs. WR14 3PS

England

+44 (0)1684 895439

Abstract

Wave wire data from the large wind-wave tank of the Ocean Engineering laboratory at the University of California, Santa Barbara are analyzed and comparisons made with published data collected in four other wave tanks. The behaviour of wind waves at various fetches (from 7 m to 80 m) is very similar to the behaviour observed in the other tanks. When the non-dimensional frequency, F^* , or non-dimensional significant wave height, H^* , are plotted against non-dimensional fetch, x^* , then a large scatter in the data points is found. Multi-variate regression to the dimensional parameters shows that H_{sig} is a function of $U^2 x$ and F is a function of $U^{1.25} x$, with the result that in general for wind waves at a particular fetch in a wave tank, approximately speaking the wave frequency is inversely proportional to the square root of the wind speed, and the wavelength is proportional to the wind speed. Similarly, the wave height is proportional to $U^{1.5}$, and the orbital velocity is proportional to the wind speed, U . Comparison with field data indicates a transition from this fetch law to the conventional one (JONSWAP) for longer fetch. Despite differences in the fetch relationship, for the wave tank and the field data, the wave height and wave period satisfy Toba's 3/2 power law. This law imposes a strong constraint on the evolution of wind wave energy and frequency; consequently the energy and momentum retention rate are not independent. Both retention rates grow with wind speed and fetch, at the short fetches present in the wave tank. The observed retention rates are completely different from those typically observed in the field, but the same constraint (Toba's 3/2 law) holds true.

1. Introduction

Waves grow in the presence of wind, as long as the wind speed is greater than the phase velocity of the waves. The wave height and hence energy of the waves and the wavelength increase with the

wind speed and the fetch. Empirical fetch laws have been sought to describe sea state as functions of the wind speed and fetch in non-dimensional form. Wilson (1965) was one of the first to provide fetch formulae and more recent examples include Kahma and Calkoen (1992) and Battjes et al (1987), which is based on the influential JONSWAP results of Hasselmann et al (1973). Komen et al. (1994) also discuss various fetch laws. Dimensional analysis that leads to the derivation of these fetch laws are provided in the pioneering works of Tulin (1996) and Fontaine (2001). Donelan et al (1992) have called into question the idea of a universal fetch-limited growth law. Badulin et al (2007) suggest that wave growth depends only on the rate of dissipation determined locally, and the law does not depend on external attributes such as wind speed at all.

It is conventional when analyzing wave data to use non-dimensional units, where wind speed and the acceleration due to gravity are used to non-dimensionalise the various quantities such as frequency and wave height. When the wave wire data from the University of California Santa Barbara (UCSB) wave tank were first examined using non-dimensional quantities, there was a very wide scatter in the data points, which was not necessarily present when dimensional values were used. As a result, this paper will use dimensional data values to derive the relationships between the wind speed, fetch and the resulting dominant wave frequency and wave height. This means that at times, inelegant fractional quantities will be plotted, but with the benefit of reducing the data spread, so that there is much less scatter observed in the graphs shown. The motivation of this study is to investigate the fetch laws for short fetch.

2. Wave tank experiment

Figure 1 shows a sketch diagram of the UCSB wave tank. Figure 2 shows the dominant frequency, F , of the wind waves measured using the OEL C-band radar at a fetch of 35 m, and discussed

elsewhere (Lamont-Smith et al, 2003). Also shown on the same graph are results published by Rozenberg et al (1999) collected using a single wave wire at a fetch of 11 m in the Scripps Institute of Oceanography (SIO) wave tank (triangle symbols), and at a fetch of 80 m in the Delft Hydraulics laboratory large wave tank (plus symbols). The lines plotted in figure 2 are all of the form $F \propto U^{-0.5}$ and fit the data well, except at the very lowest wind speeds. The wind speed was measured at a height of 50 cm in each wave tank. The data points from the three wave tanks are offset from each other as a result of the different fetches that each tank has. These results suggest that fetch laws could be found that may be generally applicable to wave tanks and short fetches.

The OEL C-band radar collects data sampled in range with a resolution of 0.0377 m. A 2-D Fourier transform of data collected with a wind speed of $U = 3.4 \text{ m s}^{-1}$ produces the $\omega-k$ diagram shown in figure 3. Overlaid on the plot are lines describing the deep water gravity wave dispersion curve,

$$\omega_n = \sqrt{nk_n g} + k_n \cdot v_{drift} \quad (1)$$

The solid line shows the gravity wave dispersion line ($n=1$) in still water. The dotted lines show the dispersion curves for the n th harmonics when the drift current, v_{drift} , is taken into account. The drift current as estimated from the data in this case is $v_{drift} = 0.06 \pm 0.01 \text{ m s}^{-1}$. Other measurements at higher wind speeds (and larger waves) suggest that the drift current measured by the radar is approximately 1% of the wind speed. The wavelength of the waves, L measured by the radar is not directly affected by the drift current and it was found to scale linearly with the wind speed, $L \propto U$. Lamont-Smith et al (2003) used the radar data to investigate the presence of wave groups and spectral downshifting with fetch in the wave tank and observed that the waves change frequency in discrete steps associated with wave breaking events. Fuchs and Tulin (2000) found that the radar data could also give an estimate of the surface height spectrum, which was comparable to wave wire spectra; here only the wave wire data will be analysed in any detail.

a. Frequency dependence

An experiment was conducted in the UCSB wave tank in 1998, where an array of 10 wires was positioned along the tank, and data was collected at five different wind speeds. The variation in the peak frequency of the measured height spectra are shown in figure 4 as a function of distance down the tank. Data from the shortest fetch (4 m) is not shown, as the measured frequency was significantly lower than expected for all wind speeds, which was probably a problem associated with the estimation of the peak frequency for the very low spectral energies present. For the higher wind speeds the fetch dependence is approximately $F \propto x^{-0.4}$ but this relationship does seem to be wind speed dependent to a certain extent.

In general, a non-dimensional fetch law for the frequency may be written as,

$$\frac{Fu_*}{g} \propto \left(\frac{xg}{u_*^2} \right)^{-\alpha} \quad (2)$$

The relationship found from the JONSWAP data (Hasselmann et al, 1973) is widely preferred in the literature, with $\alpha = 0.33$. Other empirical values of the exponent α from various observations are summarized in table 1.

The wind speed U that is used here is the average velocity in the wind tunnel 50 cm above the still water surface. The non-dimensional quantities such as F^* , H^* and x^* , where $F^* = FU/g$, $H^* = Hg/U^2$ and $x^* = xg/U^2$, are often used in plotting this kind of wind wave data. Thus equation (2) may be re-written,

$$F^* = C x^{*-\alpha}$$

(3)

where C is assumed to be a non-dimensional constant.

Figure 5 shows a scatter plot of the non-dimensional quantities, F^* versus x^* . There is a wide spread in the values, although a dotted line of the form $F^* = 3 x^{*-0.38}$ can be drawn through the large wind speed values, but this ignores the lower wind speed cases.

One way to establish the relationship between the wind speed and the fetch is to use a contour plot on log-paper showing the iso-frequencies, as in figure 6. The advantage of displaying the data in this way is that no assumption is made about the relationship between the wind speed and the fetch. The iso-frequencies seem to be parallel to the dotted lines of the form $\log[U] = -0.8 \log[x] + \text{constant}$, hence figure 7 re-plots the data against the quantity $U^{1.25} x$. For waves of frequency less than 4 Hz (or wavelengths larger than 10 cm) the data is well reproduced by a best-fit line of the form,

$$F \propto (U^{1.25} x)^{-0.43}$$

(4)

Performing a multi-variate fit gave an exponent of 1.3 ± 0.05 for U , and the overall exponent (outside the bracket) was -0.43 ± 0.01 . Thus the frequency is approximately proportional to $U^{-0.5}$, and it is approximately proportional to $x^{-0.4}$. Equation (2) may be re-arranged to show the frequency dependence on the fetch, and the wind speed

$$F \propto x^{-\alpha}$$

$$F \propto u_*^{2\alpha-1}$$

(5)

A graph of the wind exponent (for U rather than u_*) versus the fetch exponent for the non-dimensional frequency fetch law has a straight line relationship (not shown), which is defined by (5) and that must be obeyed if the non-dimensional relationship is valid. Field measurements listed in Table 1 give specific values of α . The wave tank results are some way from conforming to the non-dimensional equation relationship expected in (5). The measured frequency dependence is closest to the JONSWAP result where $\alpha = 0.33$, but differs from this non-dimensional result by a factor $(U^2 x)^{-0.1}$, which suggests in the wave tank, C is not a constant,

$$C \propto (U^2 x)^{-0.1} \quad (6)$$

There are a number of possible explanations for this result. For instance, the drift current has an influence on the measured frequency, particularly at high frequency, however the effect of drift current has been quantified in figure 3, and the influence is believed to be minimal. It is not clear whether the wind friction velocity, u_* would be better at reducing the scatter than using U . For instance, one can argue that the friction velocity should grow with fetch. The drag coefficient, C_D , for the friction velocity can depend on the wave age (Jones and Toba, 2001). Unpublished reports from previous work indicate that the evolution of the friction velocity is not straightforward in the UCSB wave tank; however the scatter of data is much larger than can be comfortably explained by differences in the drag coefficient.

b. Wave height dependence

A scatter plot of the non-dimensional quantities, H^* and x^* , in figure 8 shows a large scatter of the data points, with only a tenuous relationship that can be drawn. A dotted line of the form $H^* = 0.03 x^{*0.32}$ has been plotted in figure 8 that appears to show a limit for the large fetch values. The

formula for the non-dimensional fetch law for the wave-height has a relationship of the form,

$$H^* = D x^{*\beta} \tag{7}$$

Performing a multi-variate fit analysis similar to that performed for the frequency data suggested that re-plotting the wave height data against the quantity $U^2 x$, as in figure 9, substantially reduces the scatter in data points compared to figure 8. The straight line is of the form,

$$H_{Sig} \propto (U^2 x)^{0.75} \tag{8}$$

This demonstrates that the significant wave height is approximately proportional to $U^{1.5}$ and $x^{0.75}$. The multi-variate analysis gave the exponent outside the bracket, as 0.76 ± 0.03 and the exponent inside the brackets for U was 2.2 ± 0.2 .

The wave height dependence is consequently stronger than expected from the conventional non-dimensional equation (7), which may be re-written as

$$H_{Sig} \propto x^\beta$$

$$H_{Sig} \propto U^{2-2\beta} \tag{9}$$

Once again the measured results are closest to the JONSWAP result, where $\beta = 0.5$, but the wave height dependence differs from this non-dimensional result by a factor $(U^2 x)^{0.25}$, which suggests that like C , D is not a constant but is a function of $U^2 x$,

$$D \propto (U^2 x)^{0.25} \tag{10}$$

c. Toba's Law

Toba's 3/2 power law (Toba, 1972), relates the non-dimensional significant wave height to the frequency,

$$H^* \propto F^{*-1.5} \quad (11)$$

Equation (11) has been widely confirmed in the literature for both wave tank and open ocean data (Masuda and Kusaba 1987), and figure 10 shows that the UCSB data also conforms to Toba's 3/2 power law in that $H^* \propto F^{*-1.5}$, at least for the larger waves in the tank. Waves with wave height less than 4 mm or wave frequency greater than 5 Hz are shown by the plus symbols, and these points have been discarded in fitting the line to the data.

If the JONSWAP values for α and β are assumed, then C and D may be evaluated from (3) and (7), and these quantities are shown in figure 11. The data in figure 11 is plotted against the non-dimensional quantity $U^2 x / g \zeta^2$, where a length $\zeta = 1$ has been introduced to make the abscissa quantity dimensionless. The diamond symbols show the quantity $C^{-1.5}$ calculated from the wave frequency, and the squares show D calculated from the significant wave height. It is worth noting that Toba's law implies $H^* F^{*1.5}$ should be constant, and therefore that $\beta/\alpha = 3/2$, so that there is no x^* fetch dependence, and $H^* F^{*1.5} = C^{1.5} D = B$. As expected from the previous analysis neither C , nor D are constant. The solid lines are parallel with a gradient of 0.15 on the log-log paper, which is the relationship expected for $C^{-1.5}$ from (6), and the lines are separated by the quantity $B = 0.01$, which is close to the value estimated in figure 10. The solid line overlaid on the values of D does match the data points relatively well, where $D \propto (U^2 x / g \zeta^2)^{0.15}$. The dashed line matches the data slightly better than the solid line, and in fact shows the relationship for D from (10) based on the earlier analysis, and has a gradient of 0.25 on the log-log paper.

Combining (6) and (10) from the earlier analysis, it can be seen that some wind speed and fetch dependence should be expected to still be present,

$$H^* F^{*1.5} \propto (U^2 x)^{0.1} \quad (12)$$

Examination of the quantity $H^* F^{*1.5}$ indicate that it is approximately constant (not shown) with no clear trends with either U or x or indeed $U^2 x$ as suggested by (12). The weak dependence of $H^* F^{*1.5}$ on either U , x , or $U^2 x$, suggests that Toba's relationship is a universal law for evolving wind sea, regardless of the distinct fetch laws satisfied in the field and in the wave tank, which indicates that the solid lines in figure 13 are in fact the preferable representation of the data. The 3/2 power law (11) derives from the evolution of wave energy and momentum, as suggested by Toba (1973). Thus, what the law imposes is a constraint that relates the evolution of the energy and momentum of the wind sea. Tulin (1994) and Fontaine (2001) have analytically derived the conventional fetch laws, taking into account Toba's law. An unexpected finding of this study is that the wind waves in the tank follow fetch laws quite distinct from those in the field, and yet Toba's law is still satisfied. The wind sea regime in the wave tank therefore appears to be a transition regime from an extremely short fetch wind sea (e.g. Waseda, Toba and Tulin 2001), to the growing wind sea in the open ocean (e.g. JONSWAP).

3. Other wave tank experiments

A number of other researchers have presented wave tank data of wind waves, including, Toba (1972), Donelan et al (1985) and Rozenberg et al (1999). The average wind speed measured in each of the tanks was measured at a height of 50 cm, except for Donelan's data, which was measured at a

height of 26 cm. The equivalent speed at a height of 10 m was also given. A logarithmic wind profile under neutral stability conditions has been assumed here, to convert the wind speed data to a height of 50 cm. This gave a small percentage change (approximately 10%) in the wind speed values compared to the 26 cm height.

The dimensional data for the wave tanks mentioned is plotted in figures 12 and 13 with frequency, F versus $U^{1.25} x$ and average wave height, H_{av} , versus $U^2 x$, respectively. In figure 12, the line is of the same form as found for the UCSB data in (4) with $F \propto (U^{1.25} x)^{-0.43}$. A multi-variate analysis of this data gives a best fit with the wind exponent of 1.4 ± 0.1 , and the overall exponent outside the brackets of -0.40 ± 0.01 , compared to the exponent of 1.3 ± 0.05 for U and -0.43 ± 0.01 found previously for the UCSB wave frequency data. The data from Donelan et al (1985) shown by the square symbols does not fit the line in figure 12 terribly closely, which accounts for the small difference in the exponent of -0.40 rather than -0.43 that was calculated.

Similarly in figure 13, the solid line is of the form $H_{av} \propto (U^2 x)^{0.75}$, just as for the UCSB results in (8). The multi-variate analysis of this data gives a best fit with the wind exponent of 2.1 ± 0.1 , and the overall exponent outside the brackets of 0.74 ± 0.02 , compared to the exponent 2.2 ± 0.1 for U and 0.76 ± 0.03 found previously for the UCSB wave height data. The agreement of the multi-variate analysis for the UCSB data and the other wave tanks is very close and within the error bars of the analysis. The conventional non-dimensional quantities (H^* and F^*) for Toba's data have been plotted elsewhere by Tokuda and Toba (1982), where they observed a large scatter in the non-dimensional quantities, particularly H^* , exactly as observed for the UCSB data in figure 8.

4. Comparison with field data

Most field measurements show non-dimensional frequency or height plotted versus the non-dimensional fetch. The fetch measurements can span many decades, while measured wind speed in the field typically varies by significantly less than even one decade. It is also very hard to find steady wind conditions, particularly over large distances. As a result, the wind speed dependence identified from the wave tank data can not easily be confirmed, or denied, using field data. An interesting experiment to do would be to collect wave data in a narrow body of water like a loch, or fjord, where the wind speed can vary in strength with time, but tends to blow consistently either up or down the loch, thereby giving consistent fetches. This would allow the wind speed dependence to be investigated out to larger fetches than is possible in wave tanks.

Figures 14 and 15 show UCSB data, along with wave data collected by Walsh et al (1989) and by Burling (1959) from the open ocean and a reservoir respectively. These data sets are unusual in that the data is presented with dimensional units rather than in a non-dimensional form, and so can be analyzed here. The UCSB wind speed values have been extrapolated to give U_{10} , the wind speed at 10 m above the water surface, so that the data may be compared with the field measurements. The waves in the paper by Walsh et al (1989) become fully developed at a certain fetch (~ 200 km), and no data beyond that fetch is shown here.

Figure 14 shows a scatter plot of H_{sig} versus the quantity $U_{10}^2 x$ for the different data sets and with a dashed line showing the JONSWAP relationship of the form $H^* = D x^{*0.5}$, where $D = 0.0017 \pm 0.0002$ is a constant. The triangles symbols are taken from Walsh et al (1989) and the asterisks are from Burling (1959). The square symbols are the UCSB data, and the solid line shows the relationship (8) found in figure 10 for the UCSB wave tank data. The wave tank data clearly exhibits different growth behaviour to that shown by the field data.

It is less easy to display the frequency data from the field and tank together. Figure 15 shows a

scatter plot of the quantity $U_{10}^{1.25} x$ versus the peak frequency of the wind waves. The dashed line is of the form $F \propto (U_{10}^{1.25} x)^{-0.33}$, which is similar to the JONSWAP result for the fetch exponent, but the exponent for the wind is different. Frequency, F , versus $(U_{10} x)^{-0.33}$ would be a straight line for the JONSWAP relationship. The Walsh data was all collected at a single wind speed, and the Burling data has a relatively limited range of wind speeds which is why this plot can show the field data without a large scatter in the data points. The solid line shows the relationship (4) found in figure 7 for the UCSB tank data.

5. Conclusions

Data from the UCSB wind wave tank has been analysed in detail. It was found that using non-dimensional scaling gives a poor representation of the data with a large scatter in the data points. Multi-variate regression showed how to reduce this scatter. H is a function of $U^2 x$ and F is a function of $U^{1.25} x$ in the wave tank environment; $H_{sig} \propto (U^2 x)^{0.75}$ and $F \propto (U^{1.25} x)^{-0.4}$ respectively. These relationships are inconsistent with the conventional non-dimensional equations used to describe wind wave growth. The behaviour of wind wave growth in four other wave tanks has also been analysed and it was found to be very similar to that observed in the UCSB tank.

The wind speed dependence in a wave tank may be approximated as follows: for a given fetch in the tank, the frequency is inversely proportional to the square root of the wind speed, and the wavelength is proportional to the wind speed. This is true except at very low wind speeds and, or, very short fetches where the effect of surface tension alters the dispersion relationship. Similarly the wave height is proportional to $U^{1.5}$ and the orbital velocity is proportional to the wind speed, U .

The UCSB results were also found to be broadly consistent with the JONSWAP relationships, $F^* =$

$C x^{*-0.33}$ and $H^* = D x^{*0.5}$ except that in the wave tank environment neither C nor D are constant, but are a function of the fetch and the square of the wind speed, $C \propto (U^2 x)^{-0.1}$ and $D \propto (U^2 x)^{0.25}$. An alternative relationship for D was also proposed with $D \propto (U^2 x)^{0.15}$, which also fit the data and was consistent with Toba's law. Despite differences in the fetch relationships for the tank and the field, the wave height and wave period satisfy Toba's 3/2 power law. The quantities C and D may be related to the momentum retention and energy retention factors, $\frac{1}{\tau} \frac{dM}{dt} \propto D^2$ and $\frac{1}{E} \frac{dE}{dt} \propto (C^{-1.5})^2$ respectively, whose derivation is discussed in the appendix. Both the momentum retention and energy retention factors increased with wind speed and fetch in the short fetch environments investigated here. At longer fetch, both factors should eventually decrease to zero, since the waves will reach equilibrium with the wind, i.e. the waves stop growing. The physical interpretation of this is that in the wave tank environment, while the dissipation rate relative to the wind pumping decreases with fetch, the rate of change of wave momentum increases with fetch. Comparisons with field data suggest that the fetch relations may gradually make a transition to the conventional JONSWAP type fetch laws at longer fetch and therefore the growth of both the momentum retention and energy retention factors should slow down and eventually decrease.

Acknowledgments

T Lamont-Smith works for QinetiQ Ltd. in Malvern, UK. He was funded by a JSPS Invitation fellowship while carrying out this research as a visiting fellow in the Ocean and Environmental Engineering Department at the University of Tokyo. Both authors previously worked at the Ocean Engineering Laboratory at UCSB and thank the director of the laboratory, Professor MP Tulin. Thanks go in particular to V. Riquelme who helped to collect the wave wire data, as well as to A. Kolaini, J. Fuchs and many other colleagues at the laboratory.

6. Appendix

The proportionality constant of the power laws can be obtained following the analysis by Toba (1972) and Tokuda and Toba (1984), which considers the balance of the energy change, dE , momentum change, dM , and phase speed c_p ,

$$dE = c_p dM + M dc_p \quad (\text{A1})$$

The exact nature of the physics that results in the loss or increase of the energy and momentum will not be considered here. To obtain an evolution equation for the energy and for the phase velocity independently, a constraint on equation (A1) needs to be imposed, as follows,

$$\frac{d \ln H^*}{d \ln T^*} = \frac{s}{2} \quad (\text{A2})$$

where $H^* = gH/U^2$ and $T^* = gT/U$, as before, and s is the local equilibrium constant, where $s = 3$ is equivalent to Toba's 3/2 law. Condition (A2) imposes a strong constraint that the waves are in local equilibrium. Under steady conditions, the rate of change of energy in fetch can be derived as

$$\frac{dE^*}{dx^*} = \frac{2s^2}{s^2 - 1} G \left(\frac{\rho_a}{\rho_w} \right) C_D \equiv \frac{D^2}{2} \quad (\text{A3})$$

where τ is the sea surface wind stress and G is the momentum retention factor, as introduced in Toba (1972),

$$G \equiv \frac{1}{\tau} \frac{dM}{dt} \quad (\text{A4})$$

Here, C_D is the drag coefficient and ρ_a and ρ_w are the density of air and water. The constant D depends on both the momentum retention factor G and on s , the local equilibrium constant.

Assuming that G is weakly dependent on the fetch, or that the waves are in local equilibrium,

equation (A3) can be integrated to give a fetch law,

$$E^* = \frac{D^2}{2} x^* \quad (\text{A5})$$

which is supported by various observational studies (Table 1).

Following a similar procedure, one can obtain an evolution equation for the phase velocity, c_p , in dimensional form,

$$\frac{\partial c_p}{\partial x} = \frac{1}{s} \left(\frac{1}{E} \frac{dE}{dt} \right) = A \frac{\dot{e}_w}{E} \quad (\text{A6})$$

where the energy retention rate A is introduced. Assuming proportionality of wind pumping, \dot{e}_w , and dissipation, D_b , A can then also be expressed as,

$$A = \frac{\dot{e}_w - D_b}{\dot{e}_w} = 1 - \frac{D_b}{\dot{e}_w} \quad (\text{A7})$$

Therefore, an increase in A indicates that the magnitude of dissipation is reducing relative to the wind pumping. As the waves grow and become equilibrated, the dissipation and wind pumping balance so the wave energy remains constant, i.e. $A = 0$. So, for longer fetch, A should decrease with fetch.

Under the assumption of proportionality of wind pumping and dissipation, equation (A6) can be rewritten utilizing the power law representation of the wave growth rate due to wind pumping, such that

$$\frac{\partial c_p}{\partial x} = \frac{1}{s} \left(\frac{1}{E} \frac{dE}{dt} \right) = \frac{1}{s} A \frac{g}{c_p} \left(\frac{U}{c_p} \right)^{1+r} \quad (\text{A8})$$

The condition $r = 0$ is equivalent to Snyder's law (Snyder, 1981), which is considered to hold for

relatively large fetches in the ocean, and for $r = 1$, it is equivalent to Plant's wind pumping law (Plant, 1982). Non-dimensionalizing (A8) and by integration, the fetch law for the non-dimensional phase velocity is obtained, once again assuming that A is weakly dependent on fetch,

$$c_p^{*3+r} = \frac{A}{s} x^* \quad (\text{A9})$$

Here, $c_p^* = c_p/U$ and which can be replaced with $F^* = 1/2\pi c_p^*$ to obtain

$$F^* = \frac{1}{2\pi} \left(\frac{A}{s} \right)^{-\frac{1}{3+r}} x^{*-\frac{1}{3+r}} \quad (\text{A10})$$

This gives an expression for C in a general form,

$$C = \frac{1}{2\pi} \left(\frac{A}{s} \right)^{-\frac{1}{3+r}} \quad (\text{A11})$$

From equations (A5) and (A10), and noting that (A5) implies $r = 0$, an expression for the constant, B , for the local equilibrium condition can be derived,

$$B = C^{1.5} D = \sqrt{\left(\frac{1}{2\pi} \right)^3 \left(\frac{s}{A} \right) \frac{4s^2}{s^2 - 1} G \left(\frac{\rho_a}{\rho_w} \right) C_D} \quad (\text{A12})$$

For the typical case when Toba's relation is satisfied ($r = 0$ and $s = 3$) the only unknown parameters are the momentum retention factor, G , and the energy retention factor, A . The quantity A in (A11) can be re-arranged to,

$$A = 3(2\pi C)^{-3} \quad (\text{A13})$$

This takes a maximum value for $A = 1$ for the no dissipation case, hence the maximum value of C is around 0.23. From the analysis leading to equation (A7), A should start decreasing as the wind wave

gets equilibrated. Figure 13 shows how $C^{-1.5}$ varies, and by extension how A varies in the wave tank. This suggests that waves in the tank exhibit a special stage of wave evolution where the dissipation rate, D_b , is actually decreasing with fetch, relative to the wind pumping, for a given wind speed.

For the momentum retention rate, equation (A4) can be rewritten as,

$$G = \frac{1}{\tau} \frac{dM}{dt} = \frac{\tau_w}{\tau} = 1 - \frac{\tau_t}{\tau} \quad (\text{A14})$$

where, τ_w is the wave-induced stress, τ_t is the turbulent stress, and τ is the total stress. The turbulent stress is responsible for generating the drift current. Figure 13 shows D increasing with wind speed and fetch, and from (A3) $G \propto D^2$. An increase in G indicates therefore, an increase in the rate of change of wave momentum, or decrease in the rate of change of the water boundary layer momentum thickness. At larger fetches than in the tank, Janssen (1989) has shown theoretically that τ_w decreases with wave age, i.e. as the waves grow with fetch, G decreases.

7. References

- Badulin, S. I., A. V. Babanin, V. E. Zakharov and D. Resio (2007), Weakly turbulent laws of wind wave growth, *J. Fluid Mech.*, 591, 339-378
- Battjes, J. A., T. J. Zitman and L. H. Holthuijsen (1987), A reanalysis of the spectra observed in JONSWAP, *J. Phys. Oceanog.*, 17, 1288-1295
- Burling, R. W. (1959), The spectrum of waves at short fetches, *Deut. Hydrogr. Zeit.*, 12(2), 45-64
- Donelan, M. A., J. Hamilton and W. H. Wui (1985), Directional spectra of wind generated waves, *Phil. Trans. R. Soc. Lond. A*, 315, 509-562
- Donelan, M., M. Skafel, H. Graber, P. Liu, D. Schwab and S. Venkatesh (1992), On the growth rate of wind-generated waves, *Atmos. Ocean*, 30, 457-478
- Fontaine, E. (2001), On the evolution of high energy wind induced ocean waves, *Proc. OMAE Conf.*, OMAE2001/S&R-2172
- Fuchs, J. and M. P. Tulin (2000), Experimental scatterer characterisation: the importance and nature of compact scatterers in LGA imaging of the ocean, emphasising micro-breakers, *RTO SET symposium, Maryland, RTO MP-60*, 9-1 – 9-14
- Hasselmann, K., T. P. Barnett, E. Bouws, H. Carlson, D. E. Cartwright, K. Enke, J. A. Ewing, H. Gienapp, D. E. Hasselmann, P. Kruseman, A. Meerburg, P. Muller, D. J. Olbers, K. Richter, W. Sell and H. Walden (1973), Measurements of wind-wave growth and swell decay during the Joint North Sea Wave Project (JONSWAP), *Deut. Hydrogr. Z.*, A8 (12), 3-96
- Hicks, B. B. (1978), Some limitations of dimensional analysis and power laws, *Boundary Layer Meteor.*, 14, 567-569
- Hwang, P. A., S. Atakturk, M. A. Sletten and D. B. Trizna (1996), A study of the wavenumber spectra of short wind waves in the ocean, *J. Phys. Oceanog.*, 26, 1266-1285
- Jones, I. S. F. and Y. Toba (2001), *Wind Stress over the Ocean*, Cambridge University Press, 307 pp.

- Kahma, K. K. (1981), A study of the growth of the wave spectrum with fetch, *J. Phys. Oceanog.*, *11*, 1503-1515
- Kahma, K. K. and C. Calhoun (1992), Reconciling discrepancies in the observed growth of wind generated waves, *J. Phys. Oceanog.*, *22*, 1389-1405
- Komen, G. J., L. Cavaleri, M. Donelan, K. Hasselmann, S. Hasselmann and P. A. E. M. Janssen (1994), Dynamics and modelling of Ocean Waves, Cambridge University Press, 554 pp.
- Lamont-Smith, T., J. Fuchs and M. P. Tulin (2003), Radar investigation of the structure of wind waves, *J. Oceanog.*, *59*, 49-63
- Lamont-Smith, T. (2004), Investigation of the variability of Doppler spectra with radar frequency and grazing angle, *IEE Proc. Radar Sonar Navig.*, *151*(5), 291-298, doi: 10.10149/ip-rsn:20040859
- Masuda A. and T. Kasuba (1987), On the local equilibrium of winds and wind waves in relation to surface drag, *J. Oceanog. Soc. Japan*, *43*, 28-36
- Mitsuyasu, H., F. Tasai, T. Suhara, S. Mizuno, M. Ohkusu, T. Honda and K. Rikiishi (1980), Observations of the power spectrum of ocean waves using a cloverleaf buoy, *J. Phys. Oceanog.*, *10*, 287-296
- Phillips, O. M. (1977), The dynamics of the upper ocean, Cambridge University Press, 344 pp.
- Rozenberg, A. D., M. J. Ritter, W. K. Melville, C. G. Gottschall and A. V. Smirnov (1999), Free and bound capillary waves as microwave scatterers: laboratory studies, *IEEE Trans. Geosci. & Remot. Sens.*, *37*(2), 1052-1065
- Toba, Y. (1972), Local balance in the air-sea boundary processes I: On the growth processes of wind waves, *J. Oceanog. Soc. Japan*, *28*, 109-121
- Tokuda, M. and Y. Toba (1982), Statistical characteristics of individual waves in laboratory wind waves II. Self-consistent similarity regime, *J. Oceanog. Soc. Japan*, *38*, 8-14
- Tulin, M. P. (1994), Breaking of Ocean waves and downshifting, Waves and Nonlinear processes, J. Grue, B. Gjevik and J. E. Weber, Kluwer Academic Publishers, 177-190
- Walsh, E. J., D. W. Hancock III and D. E. Hines (1989), An observation of the directional wave

spectrum evolution from shoreline to fully developed, *J. Phys. Oceanog.*, 19, 670-690

Waseda, T., Y. Toba and M. P. Tulin (2001), Adjustment of wind waves to sudden changes of wind speed, *J. Oceanog. Soc. Japan*, 57, 519-533

Wilson, B. W. (1965), Numerical prediction of ocean waves in the North Atlantic for December, 1959, *Deut. Hydrogr. Z.*, 18(3), 114-131

List of figure captions

Figure 1: Sketch of the wave tank at the University of California, Santa Barbara.

Figure 2: Dominant wave frequency in different wave tank environments versus wind speed. Plus signs – 80 m fetch, Delft wave tank, Squares – 35 m fetch, UCSB wave tank, Triangles – 11 m fetch, SIO wave tank.

Figure 3: ω - k plot, 2D Fourier transform of radar range-time intensity radar data. Solid line is the gravity wave dispersion relation. Dotted lines show dispersion line and its harmonic in the presence of a current.

Figure 4: Dominant wave frequency in the UCSB wave tank environment versus fetch. Plus signs – 10.3 ms^{-1} , Asterisks – 9.7 ms^{-1} , Triangles – 8.4 ms^{-1} , Diamonds – 5.7 ms^{-1} , Squares – 3.4 ms^{-1} .

Figure 5: A scatter plot of the non-dimensional quantities F^* and x^* . Plus signs – 10.3 ms^{-1} , Asterisks – 9.7 ms^{-1} , Triangles – 8.4 ms^{-1} , Diamonds – 5.7 ms^{-1} , Squares – 3.4 ms^{-1} .

Figure 6: A contour plot on log-log paper showing the lines of constant frequency calculated from the UCSB frequency data. The dotted lines are of the form $\log[U] = -0.8 \log[x] + \text{constant}$

Figure 7: A scatter plot of the quantity $U^{1.25} x$ versus the peak frequency of the wind waves. The line is of the form, $F \propto (U^{1.25} x)^{-0.43}$. Plus signs – 10.3 ms^{-1} , Asterisks – 9.7 ms^{-1} , Triangles – 8.4 ms^{-1} , Diamonds – 5.7 ms^{-1} , Squares – 3.4 ms^{-1} .

Figure 8: A scatter plot of the non-dimensional quantities H^* and x^* , with a dotted line of the form, $H^* = 0.03 x^{*0.32}$, which appears to show a limit. Plus signs – 10.3 ms^{-1} , Asterisks – 9.7 ms^{-1} , Triangles – 8.4 ms^{-1} , Diamonds – 5.7 ms^{-1} , Squares – 3.4 ms^{-1} .

Figure 9: A scatter plot of the quantity $U^2 x$ versus the significant wave height, H_{sig} , of the wind waves. The line is of the form, $H_{\text{sig}} \propto (U^2 x)^{0.75}$. Plus signs – 10.3 ms^{-1} , Asterisks – 9.7 ms^{-1} , Triangles – 8.4 ms^{-1} , Diamonds – 5.7 ms^{-1} , Squares – 3.4 ms^{-1} .

Figure 10: A scatter plot of the non-dimensional quantities H^* and F^* , with a solid line of the form

$H^* = 0.012 F^{*-1.5}$ which has the correct exponent for Toba's law. Square symbols show data points used for the line fit, with wave height greater than 4 mm and frequency less than 5 Hz, Plus symbols show the smaller waves.

Figure 11: $C^{-1.5}$ and D evaluated from the UCSB data of frequency (diamond symbols) and significant wave height (square symbols). The solid lines have a gradient of 0.15 and are separated by a factor of $B = 0.01$. The dashed line has a gradient of 0.25.

Figure 12: A scatter plot of the peak frequency of the wind waves versus the quantity $U^{1.25} x$. Plus – Toba, Triangle – SIO, Asterisk – Delft, Square – Donelan. Line is of the form, $F \propto (U^{1.25} x)^{-0.43}$.

Figure 13: A scatter plot of the average wave height of the wind waves versus the quantity $U^2 x$. Plus symbols – Toba, Triangles – SIO, Asterisks – Delft, Squares – Donelan. The line is of the form, $H_{av} \propto (U^2 x)^{0.75}$.

Figure 14: A scatter plot of significant wave height of the wind waves versus $U_{10}^2 x$. Triangles are from Walsh, Asterisks are from Burling, and Squares are the UCSB data. Solid line $H_{sig} \propto (U_{10}^2 x)^{0.75}$. Dashed line $H_{sig} \propto (U_{10}^2 x)^{0.5}$.

Figure 15: A scatter plot of frequency of the wind waves versus $U_{10}^{1.25} x$. Triangles are from Walsh, Asterisks are from Burling, and Squares are the UCSB data. Solid line $H_{sig} \propto (U_{10}^{1.25} x)^{-0.43}$. Dashed line $H_{sig} \propto (U_{10}^{1.25} x)^{-0.33}$.

Table 1: Fetch laws from various observations.

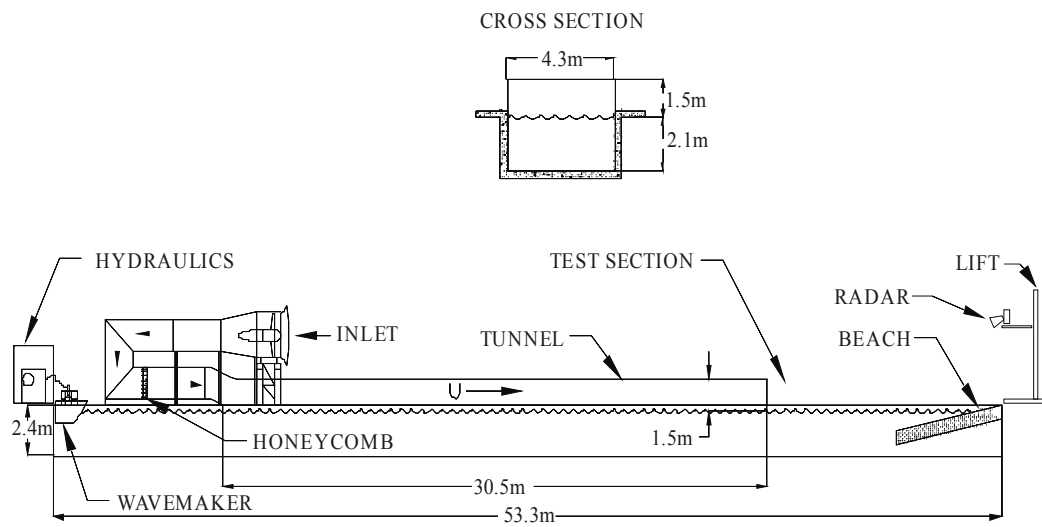


Figure 1: Sketch of the wave tank at the University of California, Santa Barbara.

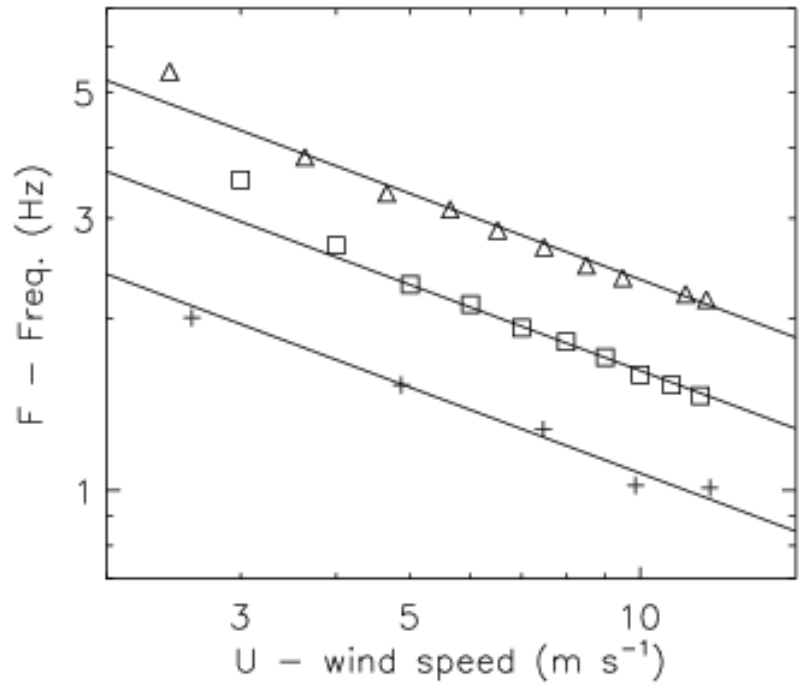


Figure 2: Dominant wave frequency in different wave tank environments versus wind speed. Plus signs – 80 m fetch, Delft wave tank, Squares – 35 m fetch, UCSB wave tank, Triangles – 11 m fetch, SIO wave tank.

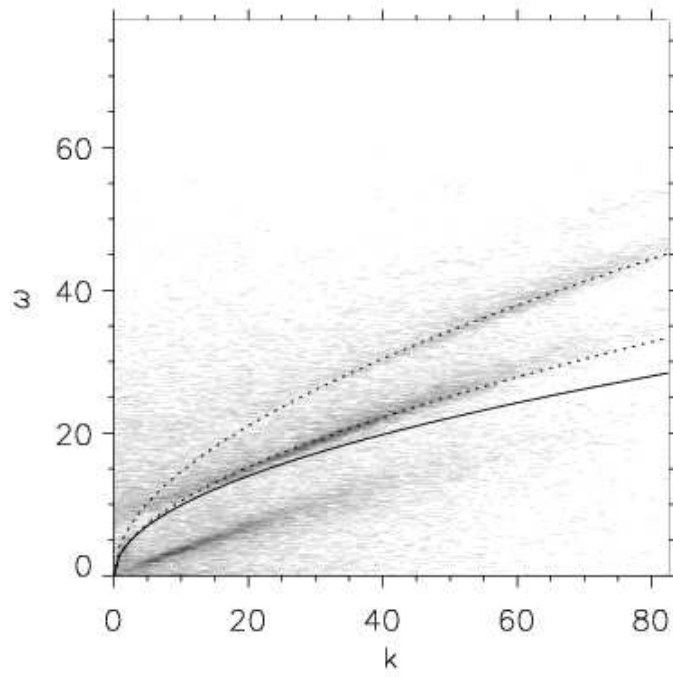


Figure 3: ω - k plot, 2D Fourier transform of radar range-time intensity radar data. Solid line is the gravity wave dispersion relation. Dotted lines show dispersion line and its harmonic in the presence of a current.

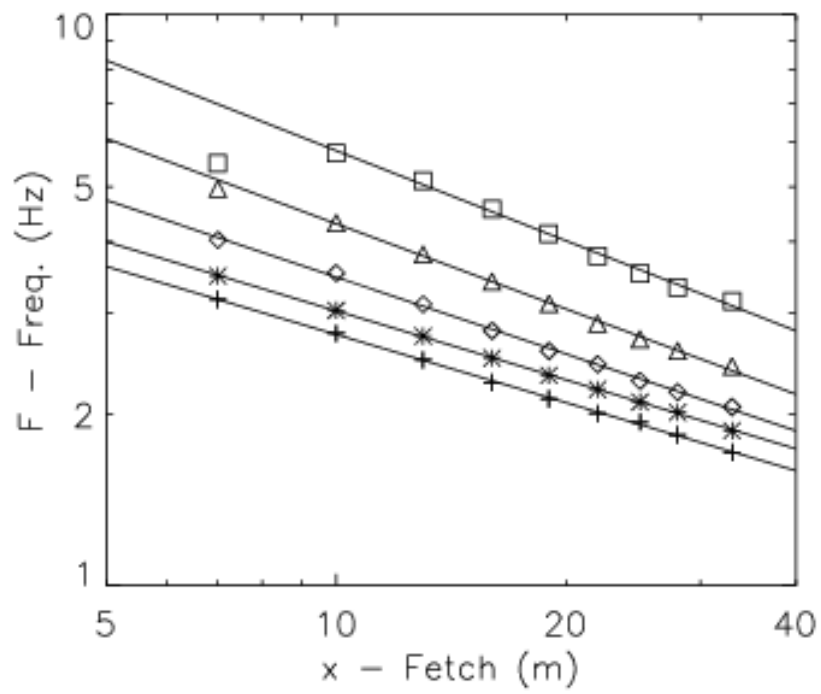


Figure 4: Dominant wave frequency in the UCSB wave tank environment versus fetch. Plus signs – 10.3 ms^{-1} . Asterisks – 9.7 ms^{-1} , Triangles – 8.4 ms^{-1} . Diamonds – 5.7 ms^{-1} . Squares – 3.4 ms^{-1} .

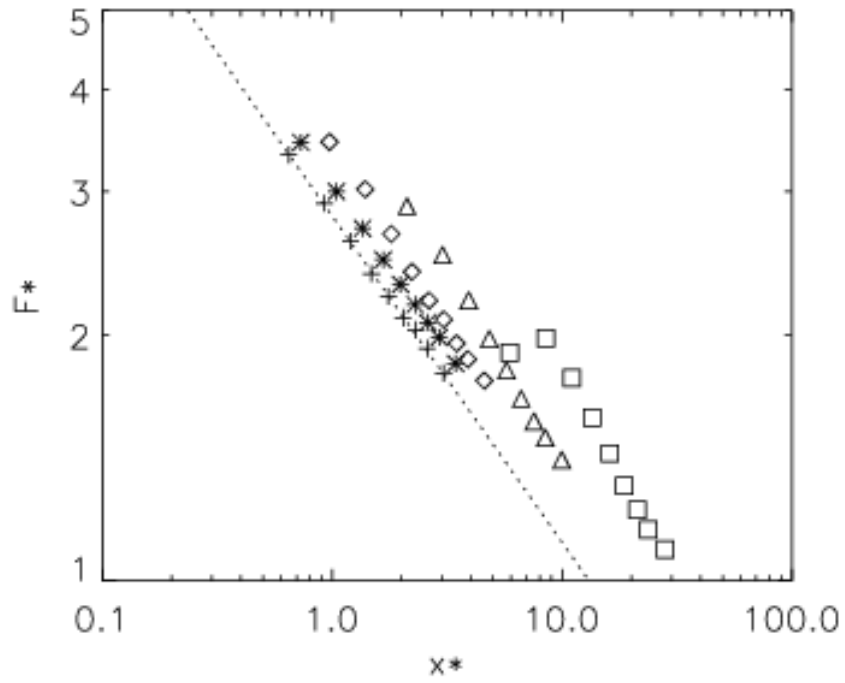


Figure 5: A scatter plot of the non-dimensional quantities F^* and x^* . Plus signs – 10.3 ms^{-1} . Asterisks – 9.7 ms^{-1} , Triangles – 8.4 ms^{-1} . Diamonds – 5.7 ms^{-1} . Squares – 3.4 ms^{-1} .

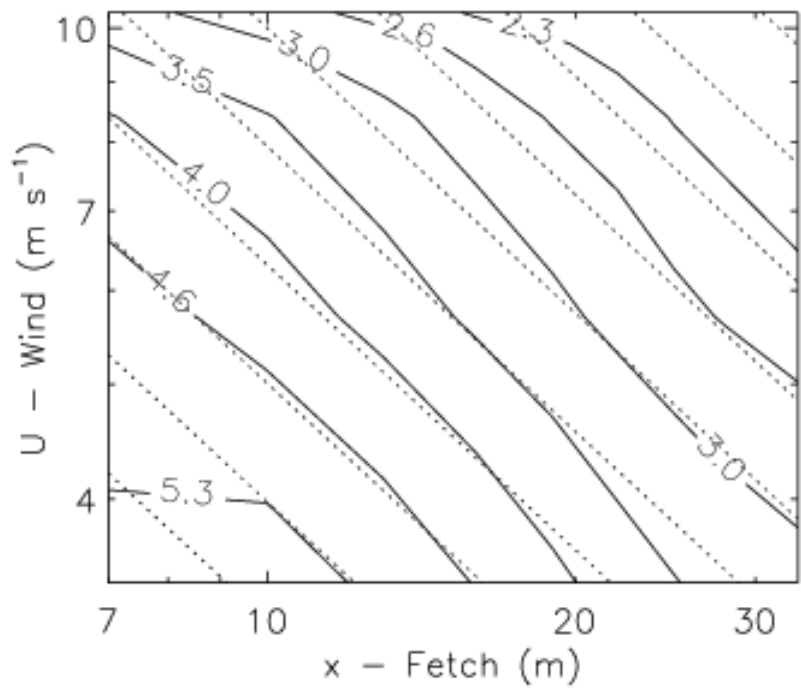


Figure 6: A contour plot on log-log paper showing the lines of constant frequency calculated from the UCSB frequency data. The dotted lines are of the form $\log[U] = -0.8 \log[x] + \text{constant}$

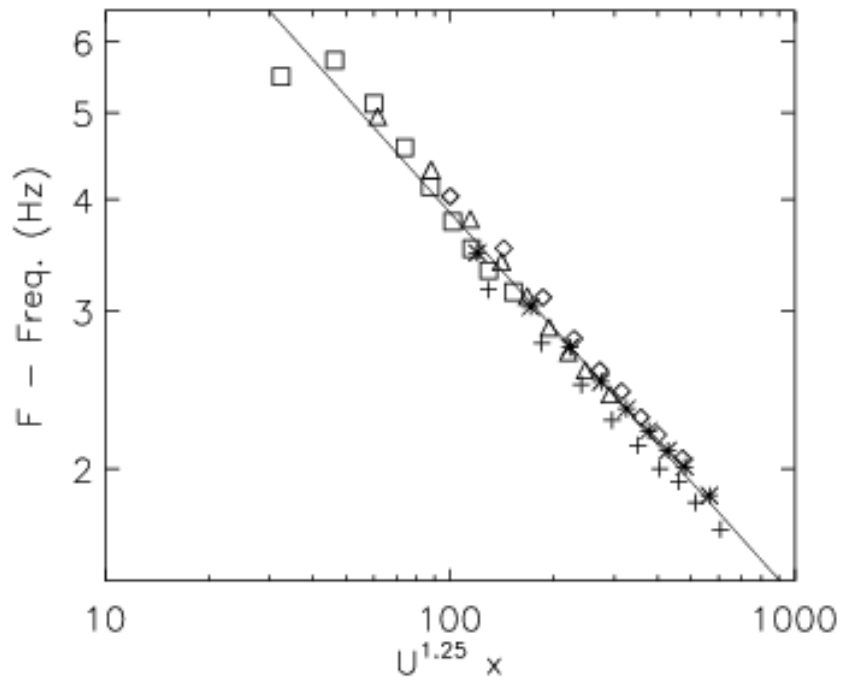


Figure 7: A scatter plot of the quantity $U^{1.25} x$ versus the peak frequency of the wind waves. The line is of the form, $F \propto (U^{1.25} x)^{-0.43}$. Plus signs – 10.3 ms^{-1} . Asterisks – 9.7 ms^{-1} , Triangles – 8.4 ms^{-1} . Diamonds – 5.7 ms^{-1} . Squares – 3.4 ms^{-1} .

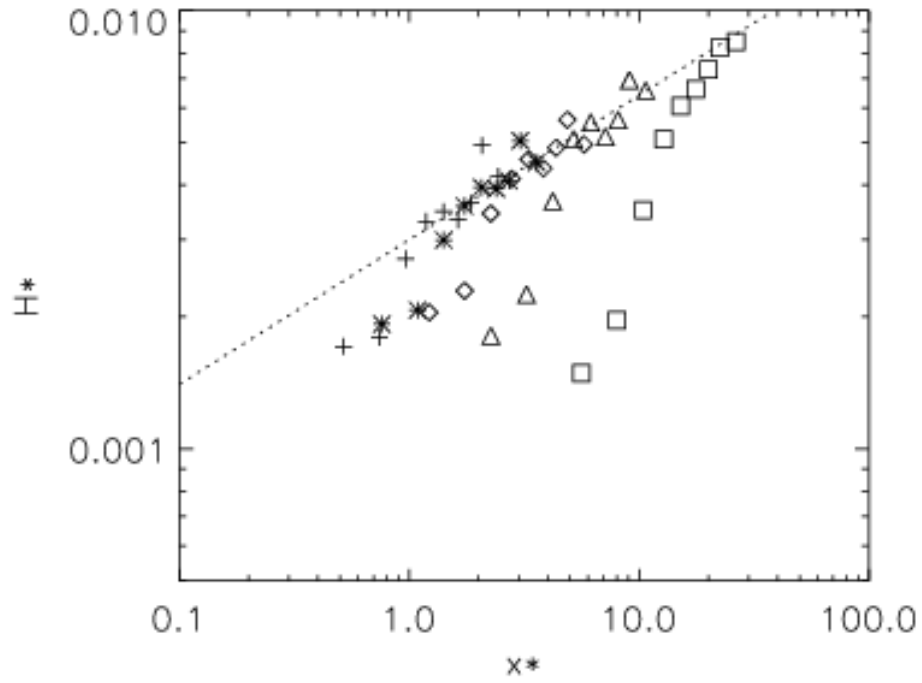


Figure 8: A scatter plot of the non-dimensional quantities H^* and x^* , with a dotted line of the form, $H^* = 0.03 x^{*0.32}$, which appears to show a limit. Plus signs – 10.3 ms^{-1} . Asterisks – 9.7 ms^{-1} , Triangles – 8.4 ms^{-1} . Diamonds – 5.7 ms^{-1} . Squares – 3.4 ms^{-1} .

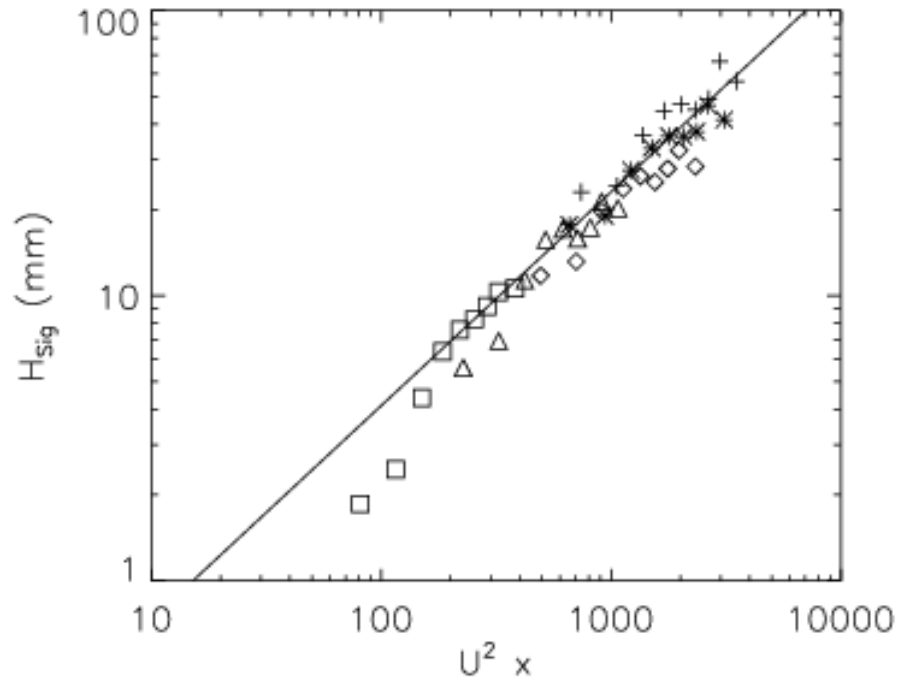


Figure 9: A scatter plot of the quantity $U^2 x$ versus the significant wave height, H_{sig} , of the wind waves. The line is of the form, $H_{\text{sig}} \propto (U^2 x)^{0.75}$. Plus signs – 10.3 ms^{-1} . Asterisks – 9.7 ms^{-1} , Triangles – 8.4 ms^{-1} . Diamonds – 5.7 ms^{-1} . Squares – 3.4 ms^{-1} .

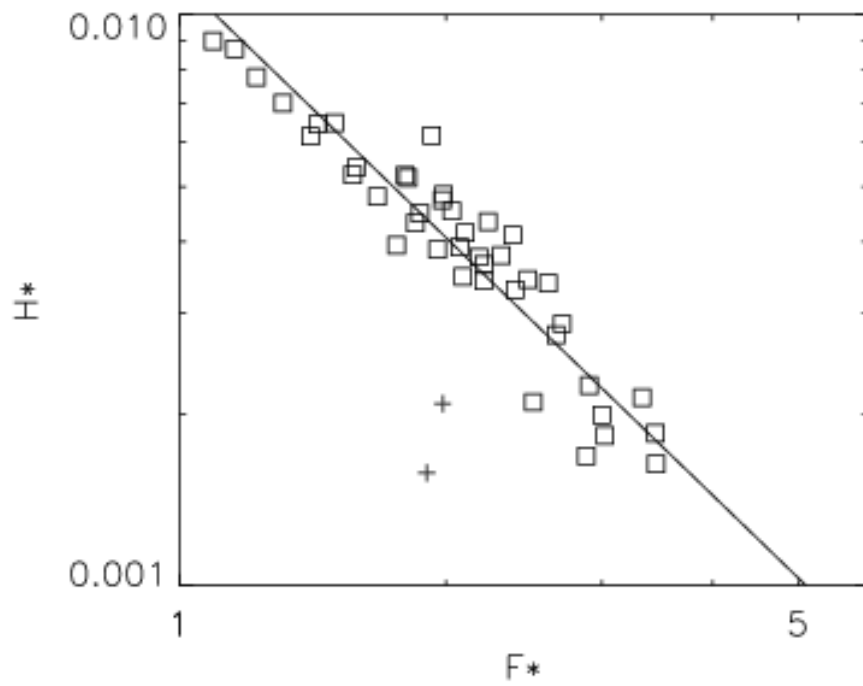


Figure 10: A scatter plot of the non-dimensional quantities H^* and F^* , with a solid line of the form $H^* = 0.012 F^{*-1.5}$ which has the correct exponent for Toba's law. Square symbols show data points used for the line fit, with wave height greater than 4 mm and frequency less than 5 Hz, Plus symbols show the smaller waves.

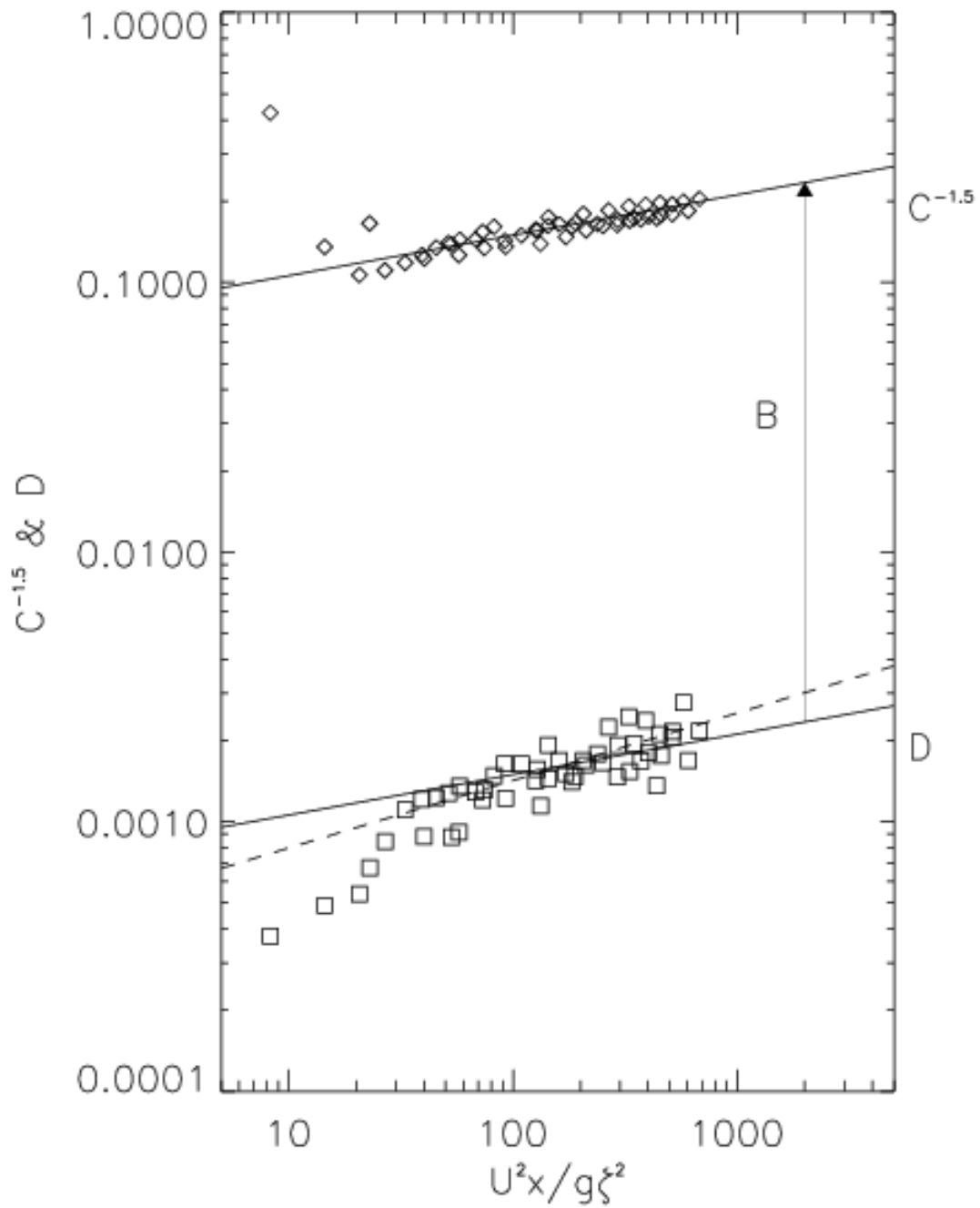


Figure 11: $C^{-1.5}$ and D evaluated from the UCSB data of frequency (diamond symbols) and significant wave height (square symbols). The solid lines have a gradient of 0.15 and are separated by a factor of $B = 0.01$. The dashed line has a gradient of 0.25.

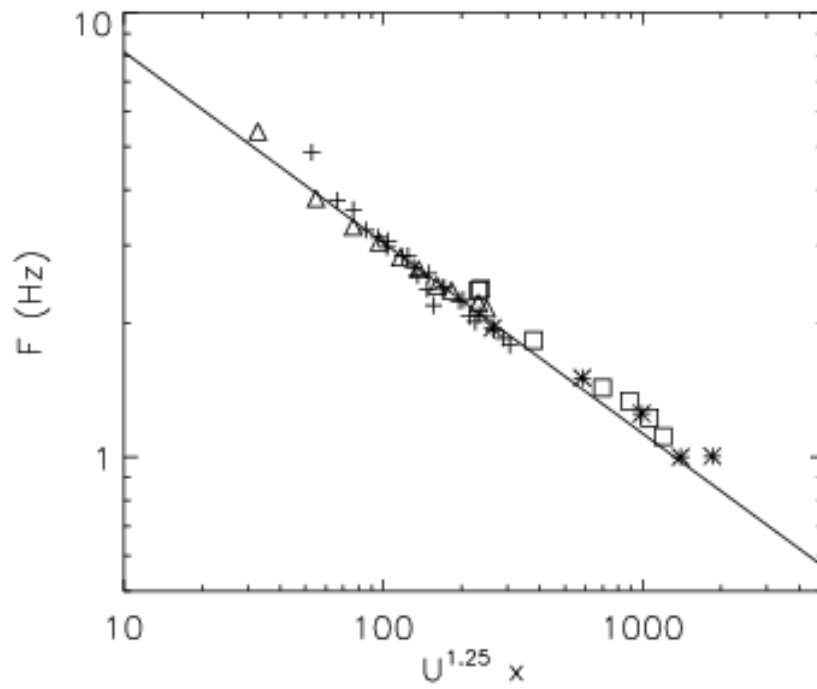


Figure 12: A scatter plot of the peak frequency of the wind waves versus the quantity $U^{1.25} x$. Plus – Toba. Triangle – SIO. Asterisk – Delft. Square – Donelan. Line is of the form, $F \propto (U^{1.25} x)^{-0.43}$.

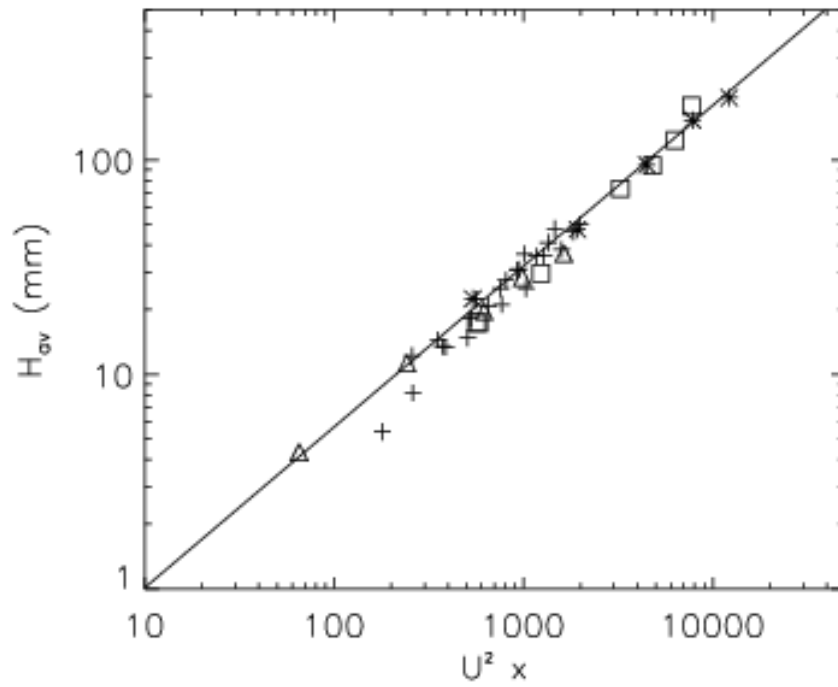


Figure 13: A scatter plot of the average wave height of the wind waves versus the quantity $U^2 x$. Plus symbols – Toba. Triangles – SIO. Asterisks – Delft. Squares – Donelan. The line is of the form, $H_{av} \propto (U^2 x)^{0.75}$.

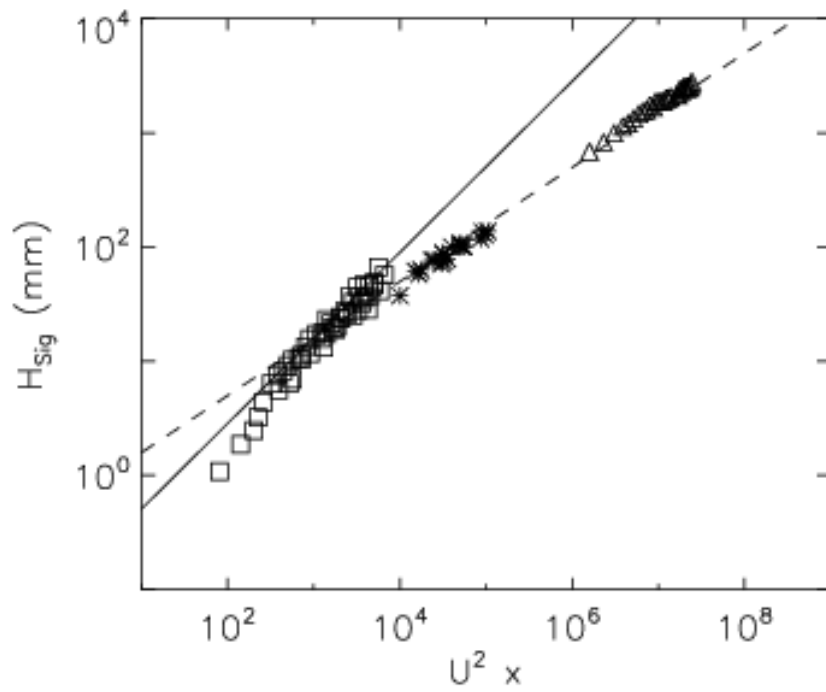


Figure 14: A scatter plot of significant wave height of the wind waves versus $U_{10}^2 x$. Triangles are from Walsh, Asterisks are from Burling and Squares are the UCSB data. Solid line $H_{sig} \propto (U_{10}^2 x)^{0.75}$. Dashed line $H_{sig} \propto (U_{10}^2 x)^{0.5}$.

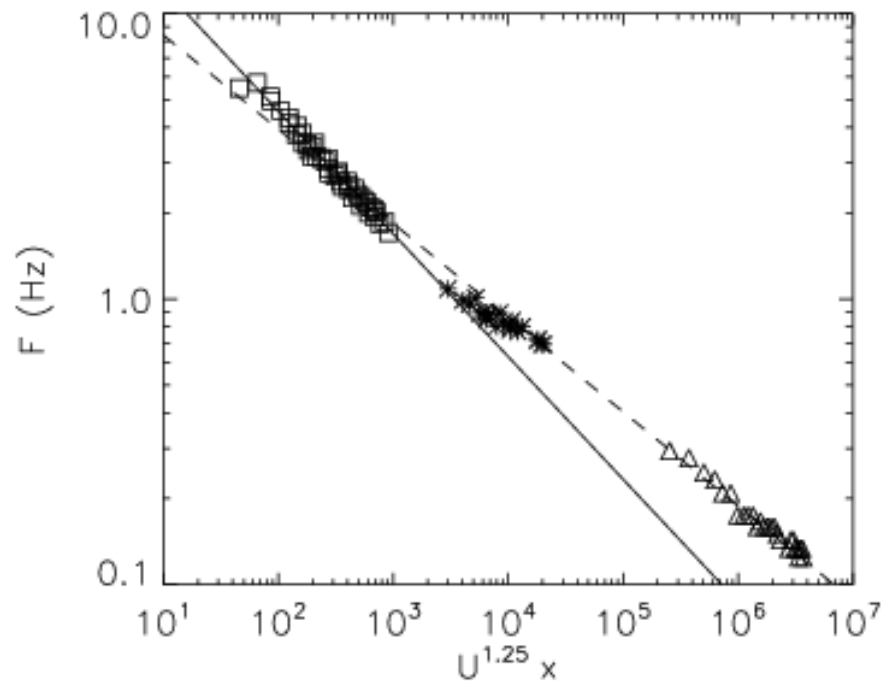


Figure 15: A scatter plot of frequency of the wind waves versus $U_{10}^{1.25} x$. Triangles are from Walsh, Asterisks are from Burling, and Squares are the UCSB data. Solid line $H_{sig} \propto (U_{10}^{1.25} x)^{-0.43}$. Dashed line $H_{sig} \propto (U_{10}^{1.25} x)^{-0.33}$.

Table 1: Fetch laws from various observations

Data set	α	β
<i>Phillips equilibrium</i>	0.25	0.5
<i>Toba's 3/2 law</i>	1/3	1/2
Donelan	0.27	0.48
Mitsuyasu	0.33	0.54
JONSWAP	0.33	0.5
Huang	0.2368	0.4053
Burling	0.225	0.427
Kahma	0.27	0.45